Geometry and edge effects on the energy levels of graphene quantum rings: A comparison between tight-binding and simplified Dirac models

D. R. da Costa,[1,2,*] Andrey Chaves,[1,†] M. Zarenia,[2] J. M. Pereira Jr.,[1] G. A. Farias,[1,‡] and F. M. Peeters[1,2]

[1]*Departamento de Física, Universidade Federal do Ceará, Caixa Postal 6030, Campus do Pici, 60455-900 Fortaleza, Ceará, Brazil*

[2]*Department of Physics, University of Antwerp, Groenenborgerlaan 171, B-2020 Antwerp, Belgium*

(Received 17 October 2013; revised manuscript received 30 January 2014; published 18 February 2014)

We present a systematic study of the energy spectra of graphene quantum rings having different geometries and edge types in the presence of a perpendicular magnetic field. Results are obtained within the tight-binding (TB) and Dirac models and we discuss which features of the former can be recovered by using the approximations imposed by the latter. Energy levels of graphene quantum rings obtained by diagonalizing the TB Hamiltonian are demonstrated to be strongly dependent on the rings geometry and the microscopical structure of the edges. This makes it difficult to recover those spectra by the existing theories that are based on the continuum (Dirac) model. Nevertheless, our results show that both approaches (i.e., TB and Dirac model) may provide similar results, but only for very specific combinations of ring geometry and edge types. The results obtained by a simplified model describing an infinitely thin circular Dirac ring show good agreement with those obtained for hexagonal and rhombus armchair graphene rings within the TB model. Moreover, we show that the energy levels of a circular quantum ring with an infinite mass boundary condition obtained within the Dirac model agree with those for a ring defined by a ring-shaped staggered potential obtained within the TB model.

DOI: 10.1103/PhysRevB.89.075418 PACS number(s): 81.05.U−, 71.10.Pm, 03.65.Ta

I. INTRODUCTION

Graphene, a two-dimensional lattice of carbon atoms [1], has been a subject of great interest during the past few years. This interest is not only due to its possible future technological applications, but also because it provides the possibility to probe interesting phenomena predicted by quantum field theories. Several of the exotic properties originate from the fact that low energy electrons in graphene obey the zero mass Dirac equation (for a review see, e.g., Ref. [2]).

Previous works have demonstrated interesting features coming from ringlike and dotlike confinement in graphene [3–9]. Theoretical studies have predicted Aharonov-Bohm (AB) oscillations in both the conductance [10] and the energy spectrum [11] of graphene quantum rings. In fact, AB conductance oscillations were observed in recent experiments on several circular rings fabricated in few-layer graphene [12]. Luo *et al*. [13] demonstrated theoretically that the energy spectrum of armchair quantum rings exhibits signatures of an effective time-reversal symmetry breaking, where a gap around zero energy, which can be removed by applying an external magnetic field, is observed.

From the point of view of the continuum model, where electrons are described as massless Dirac fermions, several models have been suggested for studying the confined states of graphene quantum rings. For instance, Recher *et al*. [14] have used the Dirac model to show that the combined effects of a ring-shaped mass-related potential and an external magnetic field can be used to break the valley degeneracy in graphene. A similar effect was also found by Wurm *et al*. [15], where it was theoretically demonstrated that the splitting of the valley degeneracy by a magnetic field in such a system can also be observed in the transport properties of rings that are weakly coupled to leads. The analytical solution for the graphene ring proposed in Ref. [14] was used latter by Abergel *et al*. [16] to study the interplay between valley polarization and electron-electron interactions on some measurable quantities in such a structure, where they observe, e.g., extra steps in the persistent current as a function of an external magnetic field. A recent paper [17] proposed a simplified model for obtaining energy levels in graphene quantum rings, based on an idea widely used for semiconductor quantum rings [18], where the radial component of the momentum of the confined particle is assumed to be zero, so that the effective Hamiltonian of the system depends only on the angular coordinate. This model has been recently used, e.g., for the study of wave packet revivals in monolayer and bilayer graphene rings [19].

Notice that the continuum model for graphene is developed by considering a periodic honeycomb lattice of carbon atoms of infinite size and by analyzing only the low energy sector of the corresponding tight-binding Hamiltonian. However, the experimentally obtained graphene quantum rings reported in the literature are normally fabricated by cutting out the graphene flake into a finite size ring-shaped structure. In order to take the finite size effects into account within the Dirac theory, the above mentioned previous papers have usually considered either infinite mass boundary conditions, or a "frozen" radial motion of the particles. But it is questionable that these conditions are really sufficient in order to describe a real graphene ring sample. If so, what are the limits of such approximations? Answering these questions is the main purpose of this paper, where we use the tight-binding model (TBM) to calculate the energy spectrum of graphene quantum rings with different geometries and different types of edges. We then discuss the main qualitative features of the obtained spectra in terms of the continuum (Dirac) approximation, making a comparison between the results obtained by such an approximation and those obtained by the TBM. Our results from tight-binding calculations show that the energy spectra

*diego_rabelo@fisica.ufc.br
†andrey@fisica.ufc.br
‡gil@fisica.ufc.br

of these systems strongly depend on the detailed structure of the edges, which makes it difficult to find analytical solutions for the energy states in these systems within the continuum model. Circular rings cut out of a graphene sheet exhibit mixed armchair and zigzag edges, and the latter leads to strongly confined edge states, which significantly affects its energy spectrum. The AB oscillations in the energy spectra for other geometries of quantum rings, where one can obtain uniform edge type, exhibit geometry-specific n-fold energy subbands, and in some cases the qualitative features of the spectrum, are shown to depend even on the alignment between inner and outer edges of the ring. Even so, we demonstrate that under specific conditions one can still use the proposed simplified model [17] to obtain analytically the main qualitative features of the energy spectra of armchair rings, or use the analytical solution proposed in Ref. [14] to observe some features exhibited by the energy spectrum obtained by the tight-binding model for a mass-related ring confinement, as we will discuss in further detail in the following sections.

The present paper is organized as follows. In Sec. II we briefly present an outline of the TBM and the investigated graphene rings. An approximate analytical solution is obtained for a simplified model within the Dirac approach in Sec. III. Our numerical results from TBM and the analytical ones from the simplified Dirac model are shown in Sec. IV. A summary and concluding remarks are reported in Sec. V.

II. TIGHT-BINDING MODEL

Graphene consists of a honeycomb lattice of carbon atoms, which can be described by the Hamiltonian

$$H_{\mathrm{TB}} = \sum_i (\epsilon_i + M_i) c_i^\dagger c_i + \sum_{\langle i,j \rangle} (\tau_{ij} c_i^\dagger c_j + \tau_{ij}^* c_i c_j^\dagger), \qquad (1)$$

where c_i ($c_i^\dagger$) annihilates (creates) an electron in site i, with on-site energy ϵ_i, and the sum is taken only between the nearest neighbors sites i and j, with hopping energy τ_{ij}. Due to the Klein tunneling effect in graphene, it is hard to confine electrons by applying an external potential [20,21]. On the other hand, a staggered site-dependent potential M_i, which is positive (negative) if i belongs to the sublattice A (B) [22], opens a gap in the energy spectrum of graphene. Due to this property, such a potential is normally used to simulate confining structures in graphene, such as quantum dots [23] and rings [14], within the Dirac model, where it appears as a mass-related term. Recent papers have suggested a way to realize such a potential experimentally, namely, by depositing the graphene lattice over specific substrates [24–26]. The effect of an external magnetic field can be introduced in the TB model by including a phase in the hopping parameters according to the Peierls substitution $\tau_{ij} \rightarrow \tau_{ij} \exp[i \frac{e}{\hbar} \int_j^i \vec{A} \cdot d\vec{l}]$, where $\vec{A}$ is the vector potential describing the magnetic field [27,28]. In the presence of a perpendicular magnetic field $\vec{B} = B\hat{z}$, we conveniently choose the Landau gauge $\vec{A} = (0, Bx, 0)$, so that the Peierls phase becomes zero in the x direction and $\exp[i \frac{2\pi x}{3a} \frac{\Phi}{\Phi_0}]$ in the y direction, where $a = 1.42$ Å is the lattice parameter of graphene, $\Phi_0 = h/e$ is the magnetic quantum flux, and $\Phi = 3\sqrt{3}a^2 B/2$ is the magnetic flux through a carbon hexagon.

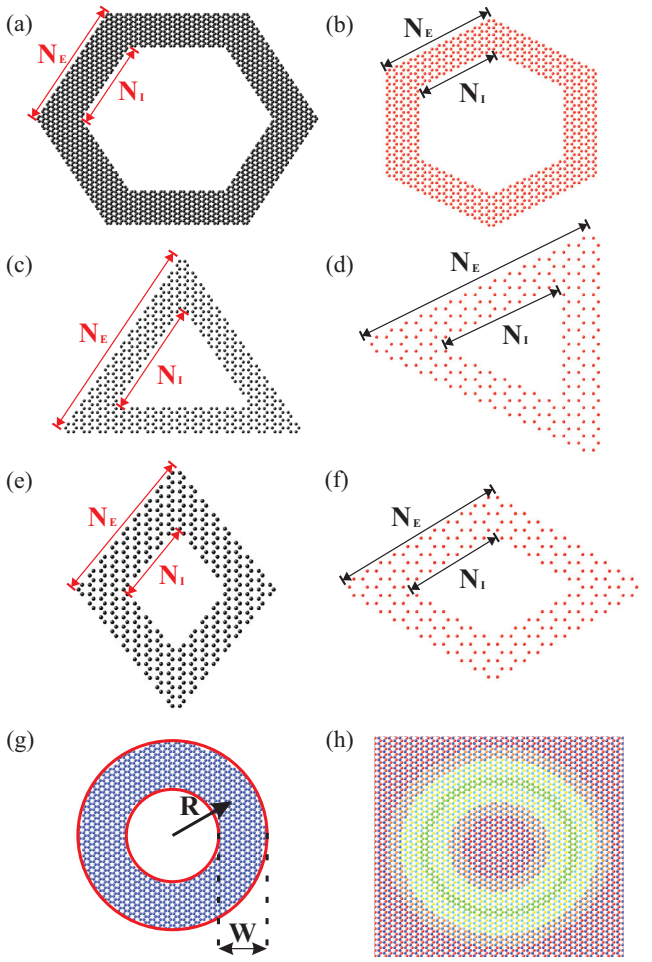

FIG. 1. (Color online) Sketch of (a), (c), and (e) armchair and (b), (d), and (f) zigzag rings, with hexagonal, triangular, and rhombus geometries, respectively, as well as (g) and (h) circular rings, considered in this work. The first six geometries are characterized by the number of carbon rings N_E (N_I) in their outer (inner) edge. Circular rings are characterized by their width W and average radius R. (g) Circular ring defined by cutting the graphene lattice. (h) Circular graphene ring defined by a smooth ring-shaped staggered potential M_i, where the color scale goes from $M_i = -M_0$ (red) to $M_i = +M_0$ (blue), and the $M_i = 0$ region inside the ring is represented in green. The atoms belonging to sublattices A and B have different colors because of the staggered potential profile.

We write the Hamiltonian (1) in matrix form, diagonalize it numerically, and obtain the energy spectrum for the different ring geometries schematically shown in Fig. 1: hexagonal, triangular, and rhombus-shaped rings, with armchair [Figs. 1(a), 1(c), and 1(e)] and zigzag [Figs. 1(b), 1(d), and 1(f)] edges. We also consider circular rings defined by cutting the graphene lattice [Fig. 1(g)], or by considering a circular-shaped staggered potential [Fig. 1(h)]. The edges of such circular rings exhibit an admixture of zigzag and armchair regions and are not singly defined. The ring-shaped staggered potential in Fig. 1(h) is given by

$$M_i(r_i) = \pm M_0[2 + \tanh(r_i^+) + \tanh(r_i^-)], \qquad (2)$$

where $r_i^+ = (r_i - R - W/2)/S$ and $r_i^- = (-r_i + R - W/2)/S$, S is the width of the smooth region and $r_i = \sqrt{x_i^2 + y_j^2}$ is the

position of the ith site of the lattice. Such a staggered potential goes smoothly to zero (M_0) inside (outside) the ring region, avoiding edge-related effects.

Probability density currents within the TB model are numerically calculated based on the method developed in Ref. [29], where one defines the probability current $\vec{j}$ in terms of the continuity equation and, after some calculations, obtain the current components in x and y directions for each site, which is defined by its line (n) and column (m) position in the lattice (see Ref. [30]), as

$$\begin{aligned} j_x(n,m) = \pm\frac{a}{\hbar}\{&2\mathrm{Im}[\Psi_{n,m}\Psi^*_{n,m\pm1}\tau_{n,m\pm1}] \\ &- \mathrm{Im}[\Psi_{n,m}\Psi^*_{n-1,m}\tau_{n-1,m}] \\ &- \mathrm{Im}[\Psi_{n,m}\Psi^*_{n+1,m}\tau_{n+1,m}]\} \end{aligned} \tag{3}$$

and

$$\begin{aligned} j_y(n,m) = \frac{\sqrt{3}a}{\hbar}\{&\mathrm{Im}[\Psi_{n,m}\Psi^*_{n+1,m}\tau_{n+1,m}] \\ &- \mathrm{Im}[\Psi_{n,m}\Psi^*_{n-1,m}\tau_{n-1,m}]\}, \end{aligned} \tag{4}$$

where the $\mp$ sign in j_x will be positive (negative) if the (n,m) site belongs to the sublattice A (B), and $\tau_{n,m}$ is the hopping parameter which, in the presence of a magnetic field, includes an additional phase according to the Peierls substitution.

III. CONTINUUM MODEL

The energy spectrum of an infinite graphene sheet in the absence of external potentials and magnetic field, as obtained from the TBM Hamiltonian (1), is gapless in six points of the reciprocal space, from which only two are inequivalent, labeled as K and K' [2,31]. In the vicinity of each of these points, the energy depends linearly on the wave vector $\vec{k}$ and the electron behaves as a quasiparticle described by the Dirac Hamiltonian

$$H_D = [v_F\vec{\sigma}(\vec{\mathbf{p}} + e\vec{A}) + V(\vec{r})\mathbf{I} + \gamma M(\vec{r})\sigma_z], \tag{5}$$

where $v_F = 3\tau a_0/2\hbar$ is the Fermi velocity, $\vec{A}$ is the electromagnetic vector potential, $V(x,y)$ is an external potential, $\mathbf{I}$ is the identity matrix, and $\vec{\sigma}_i$ denotes the components of the Pauli matrices. The eigenstates of the Hamiltonian (5) are the two-component spinors $\Psi = [\Psi_A, \Psi_B]^T$, where $\Psi_{A(B)}$ are the envelop functions associated with the electron probabilities in $A(B)$ sublattices.

The site-dependent staggered potential M_i in the TB Hamiltonian (1) contributes to the Dirac Hamiltonian as a mass-related potential $M(\vec{r})$, which is multiplied by a factor $\gamma = 1$ (-1) for the K (K') Dirac point in Eq. (5). Considering the mass as zero (infinity) inside (outside) of the confinement region yields the infinity-mass boundary condition $\Psi_B(\vec{r})/\Psi_A(\vec{r}) = i\gamma e^{i\theta}$, where θ is the angle between the outward unit vector at the boundaries and $\vec{r}$ [i.e., $\theta = 0$ $(\theta = \pi)$ at outer (inner) boundaries of the ring] [32].

Let us now consider a simplified model of a circular graphene ring in order to find an approximate analytical solution for the energy spectrum of graphene quantum rings that agrees with those obtained within the TBM. In the absence of an external potential and around the K point ($\gamma = 1$) [33], the Hamiltonian (5) in polar coordinates reads

$$H_D = \hbar v_F \begin{bmatrix} \frac{M}{\hbar v_F} & -i\left(\Pi_r^* + e^{-i\phi}\frac{\pi r B}{\Phi_0}\right) \\ -i\left(\Pi_r - e^{i\phi}\frac{\pi r B}{\Phi_0}\right) & -\frac{M}{\hbar v_F} \end{bmatrix}, \tag{6}$$

where $\Pi_r = e^{i\phi}(\frac{\partial}{\partial r} + \frac{i}{r}\frac{\partial}{\partial\phi})$. We assume that the width of the ring approaches zero and therefore the momentum should be frozen in the radial direction. From the definition of the radial momentum operator [34] in cylindrical coordinates

$$\mathbf{p}_r = \frac{1}{2}(\mathbf{p}_r\cdot\hat{\mathbf{r}} + \hat{\mathbf{r}}\cdot\mathbf{p}_r) = \frac{\partial}{\partial r} + \frac{1}{2R}, \tag{7}$$

where $\hat{\mathbf{r}}$ is the unitary vector in the radial direction and R is the ring radius, we obtain $\partial/\partial r \to -1/2R$, as $\hat{p}_r \to 0$ and $r \to R$. Then, the simplified Hamiltonian for the graphene quantum ring is

$$H_D = \begin{bmatrix} \bar{M} & -e^{-i\phi}\left(\frac{d}{d\phi} + i\frac{\Phi_R}{\Phi_0} - \frac{i}{2}\right) \\ e^{i\phi}\left(\frac{d}{d\phi} + i\frac{\Phi_R}{\Phi_0} + \frac{i}{2}\right) & -\bar{M} \end{bmatrix}, \tag{8}$$

where $\Phi_R = \pi R^2 B$ is the magnetic flux through the quantum ring, and the energy is in units of $E_0 = \hbar v_F/R$ and $\bar{M} = M/E_0$.

Notice that the definition of the radial momentum in Eq. (7) was first used by Aronov and Lyanda-Geller [35] in 1993 for the study of Schrödinger electrons in a quantum ring with Rashba spin-orbit interaction [2]. However, they mistakenly defined the radial momentum as $\mathbf{p}_r = \frac{\partial}{\partial r}$, which leads to $\frac{\partial}{\partial r} \to 0$ as the radial momentum approaches zero. Due to this wrong assumption, they ended up with a non-Hermitian Hamiltonian for this system. The non-Hermiticity of this Hamiltonian was eliminated *artificially* in subsequent papers [36,37] by assuming an additional term $-1/2R$ in the off-diagonals of the Hamiltonian. A physical explanation for such a term was given almost 10 years later in a work by Meijer *et al.* [18], where the authors split the Hamiltonian into two parts, one for the radial confinement and the other for the Rashba interaction, and used the eigenfunctions of the radial part to show that the average value of the radial first derivative term in the Rashba Hamiltonian is $\langle\partial/\partial r\rangle = -1/2R$. However, this is not the most general way to explain this term and such an explanation does not help for the graphene ring Hamiltonian (6), since in this case we cannot split the Hamiltonian and obtain a separate radial confinement term. Using Eq. (7), on the other hand, one obtains the result found by Meijer *et al.* in a more natural way, showing that the identity $\langle\partial/\partial r\rangle = -1/2R$ is actually a consequence of the zero radial momentum. Our derivation of the graphene ring Hamiltonian in Eqs. (6)–(8) shows that if one simply defines the radial momentum properly, the correct expression for the radial derivatives and, consequently, an Hermitian Hamiltonian will appear naturally from the derivation. It is straightforwardly seen that the same happens in the derivation of the Rashba interaction Hamiltonian for quantum rings.

The eigenstates of the Hamiltonian (8) are found as $\Psi_l = [A_l e^{il\phi}, \quad iB_l e^{i(l+1)\phi}]^T$, with eigenenergies

$$E = \pm\sqrt{\left(l + \frac{\Phi_R}{\Phi_0} + 1\right)\left(l + \frac{\Phi_R}{\Phi_0}\right) + \frac{1}{4} + \bar{M}^2}, \qquad (9)$$

where l is the angular momentum index.

IV. RESULTS AND DISCUSSION

A. Comparison between tight-binding and Dirac models

First, let us investigate the energy spectrum of graphene quantum rings, with various shapes and edge types, obtained by the TBM, focusing on the search for energy spectra that can be satisfactorily described by the continuum model. With this purpose, we first demonstrate that for a rhombus-shaped ring with armchair edges, a strong dependence of the energy spectrum on the edge alignment is observed in Fig. 2 for $N_E = 17$, considering $N_I = 12$ [Fig. 2(a)], where the inner and outer edges are anti-aligned, and $N_I = 11$ [Fig. 2(b)], where the edges are aligned. In the former case one obtains very regular oscillations as the magnetic field increases, for a wide range of energies. High and irregular energy differences between the excited states are found in the latter (aligned) case, as compared to the smaller and more regular separations between energies of the eigenstates of the system with anti-aligned edges. In both cases, the spectrum exhibits twofold bands of oscillating energies, separated by anticrossings, even in the higher energy region, as shown in the insets.

Figure 3 shows that hexagonal armchair quantum rings also share the same kind of spectrum as the anti-aligned armchair rhombus-shaped ring in Fig. 2(a), though in the hexagonal case the spectrum does not depend on the edges alignment, but only on the ring width. The spectra exhibit crossings and anticrossings, which separate them into sixfold energy bands. A similar spectrum was also obtained in Ref. [38], but the focus of this previous work was on the inner and outer edge distribution of the eigenfunctions, so that details of the spectrum, e.g., its dependence on the ring width and the persistent current profile of the energy states at nonzero magnetic field, were not investigated. Notice that changing the number of carbon hexagons in the inner edge N_I and

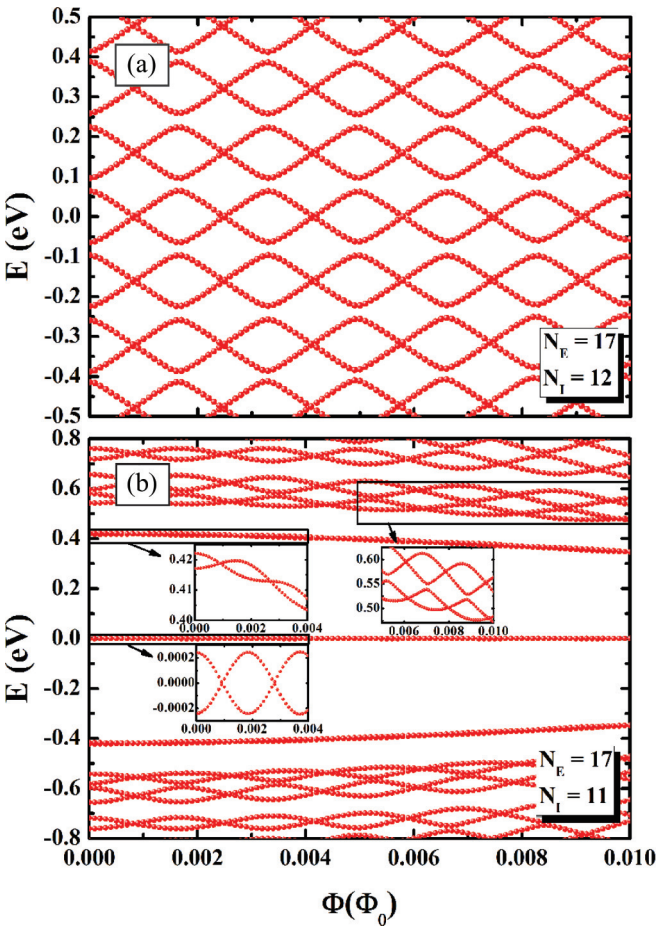

FIG. 2. (Color online) Energy levels of armchair rhombus quantum rings, schematically shown in Fig. 1(e), as a function of the magnetic flux through a single carbon hexagon for two ring widths: (a) $N_E = 17$, $N_I = 12$ and (b) $N_E = 17$, $N_I = 11$. As shown in the insets, the energy spectrum does not have a zero-energy state: States close to $E = 0$ are rather similar to the first states above and below this energy, which are composed by branches of two oscillating energy states.

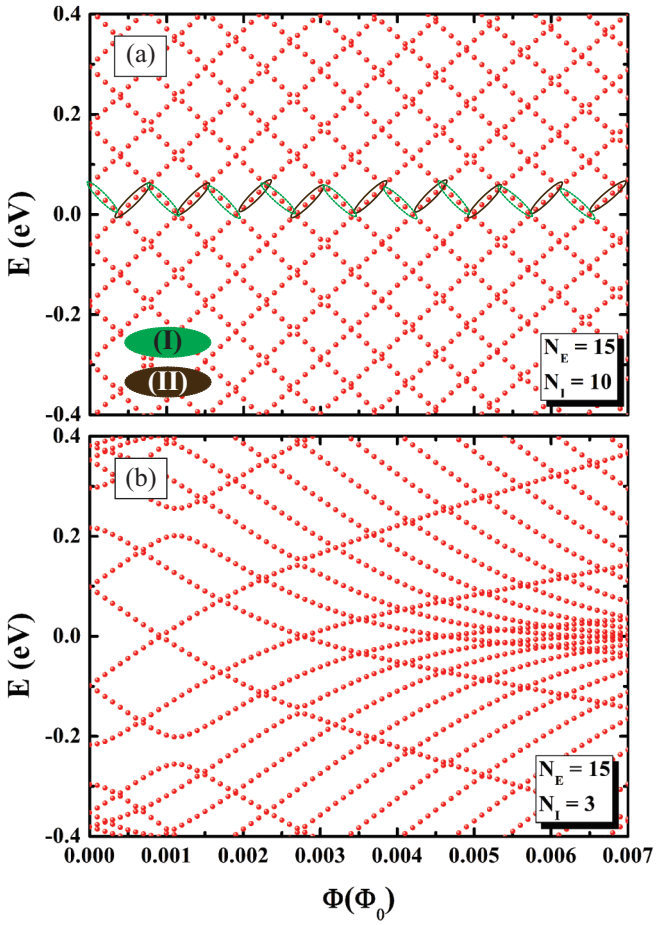

FIG. 3. (Color online) Energy levels of armchair hexagonal quantum rings, schematically shown in Fig. 1(a), as a function of the magnetic flux through a single carbon hexagon for two ring widths: (a) $N_E = 15$, $N_I = 10$ and (b) $N_E = 15$, $N_I = 3$. The spectrum is symmetric with respect to $E = 0$.

keeping N_E fixed, one effectively changes the width of the ring. Considering a larger ring width, with $N_E = 15$ and $N_I = 3$, as shown in Fig. 3(b), the energy spectrum is more strongly affected by the magnetic field, so that the regular set of crossings and anticrossings in Fig. 3(a) is no longer observed in this case. Nevertheless, the qualitative features observed in Fig. 3(a), including the gap around $E = 0$ for zero magnetic field, are present for all ring widths. This is surprising, since in armchair nanoribbons the character of the system oscillates between metallic and insulating as the width changes [39]. Although the armchair ring in Fig. 3(a) is made just by connecting six armchair nanoribbons, the qualitative features of such ribbons are not directly transferable to the quantum ring case, which suggests that the ring geometry and the ribbons connections are playing a major role in these systems [13].

Notice that the energy spectra obtained by the TBM either in the case of a rhombus-shaped armchair ring with anti-aligned edges in Fig. 2(a), or for hexagonal armchair rings, specially the one with smaller width in Fig. 3(a), resembles the AB oscillations for ideal quantum rings reported, e.g., in Fig. 3(a) of Ref. [17]. These structures are then good candidates to be well described by the simplified Dirac model for quantum rings, developed in Sec. II of the present paper and in Ref. [17].

Thus, let us investigate the spectra in Figs. 2(a) and 3(a) with more details. Notice that both spectra exhibit a gap around $E = 0$ in the absence of a magnetic field, but the $E = 0$ states are found for specific values of the magnetic flux, which are almost equally spaced in flux. This is reminiscent of the energy spectrum for Schrödinger electrons confined in quantum rings under perpendicular magnetic fields [40–42], where the energy oscillates periodically with the magnetic flux, due to the Aharonov-Bohm effect. Similar to the AB effect in semiconductor quantum rings, the energy oscillations in Fig. 3(a) can also be linked to transitions between states with clockwise and counterclockwise persistent currents, as one can observe in the probability density current plots in Fig. 4. The current for the lowest energy state with decreasing (increasing) energy as the magnetic field increases, which are marked by green (brown) ellipses labeled as I (II) in Fig. 3(a), are found to be in (counter-)clockwise direction in Fig. 4.

As a matter of fact, assuming a Dirac fermion constrained to move in a circle that is thread by the same magnetic flux as the rhombus or the hexagon, i.e., that encloses the same area as these geometries, as illustrated in Figs. 5(a) and 6(a), respectively, and performing the analytical calculations for AB oscillations in the continuum model proposed in Sec. III, one obtains almost the same spectra as obtained by the TBM for the respective structures. This is demonstrated in Figs. 5(b) and 6(b) for the rhombus-shaped and hexagonal rings, respectively, where the dashed lines are obtained by the TBM, whereas the solid lines are for a massless Dirac fermion in a circle of radius R. By comparing both models, one observes that (i) the energy gap reaches a maximum value $E = \hbar v_F/R$ at $\Phi_R = n\Phi_0$ (n integer) and (ii) the system is gapless for $\Phi_R = (n + 1/2)\Phi_0$. Better agreement between the models is observed for lower energies and magnetic fields, where the effects of the curvature of the energy bands and the finite width of the TBM sample are less important.

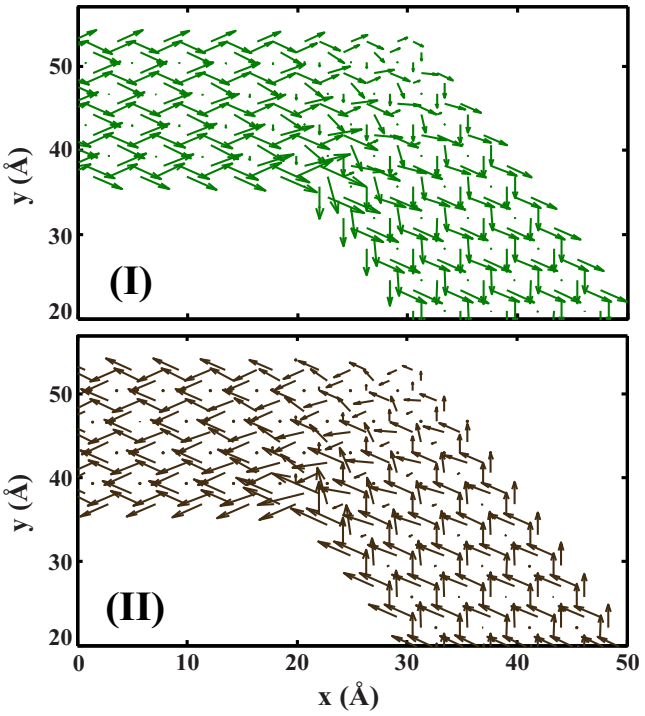

FIG. 4. (Color online) Current density profile for an armchair hexagonal quantum ring corresponding to magnetic flux indicated by (I) and (II) in Fig. 3(a). The results for the current density are numerically calculated based on the method discussed in Refs. [29,43] and reproduced in the present paper.

The main advantage of the simplified analytical model for these systems is to predict effects and results just by analyzing the solutions of the model, without effectively solving the TBM equation, which may require high computational costs. Let us then consider the case of a ring deposited over a substrate that provides a constant mass-related potential $M = 0.5E_0$. Notice that this is still not the case proposed in Fig. 1(h), since in the present case we have a constant mass term M, instead of the space-dependent potential $M_i(r_i)$ of Eq. (2). The simplified model for a $M = 0.5E_0$ in a circle of radius R predicts that such a mass term is responsible for a minimum gap of E_0 in the energy spectrum at $\Phi_R = (n + 1/2)\Phi_0$, as shown by the solid lines in Figs. 5(c) and 6(c) for the rhombus-shaped and hexagonal rings, respectively. Such prediction is indeed confirmed by the results from the TBM (dashed lines) for the respective site-dependent potentials, which exhibit very good agreement with the continuum model results.

The simplified continuum model also predicts that, in the absence of magnetic field, the energy levels converge to $\bar{M}$ as the ring radius is enlarged, and diverge as $E \approx v_F\hbar|l + 1/2|/R$ for small radii, which can be inferred from Eq. (9). However, for nonzero magnetic field, the energies are expected to increase almost linearly with the radius, since Eq. (9) can be approximated by $E = \sqrt{(\alpha R)^2 + M^2}$, with $\alpha = v_F eB/2$, as $R \to \infty$ in this case. This is illustrated by the solid lines in Fig. 7, which represent the energy levels, obtained by the simplified continuum model, as a function of the ring radius, for a circular ring with a substrate induced potential $M =$ 0.1 eV, considering different values of magnetic flux. The

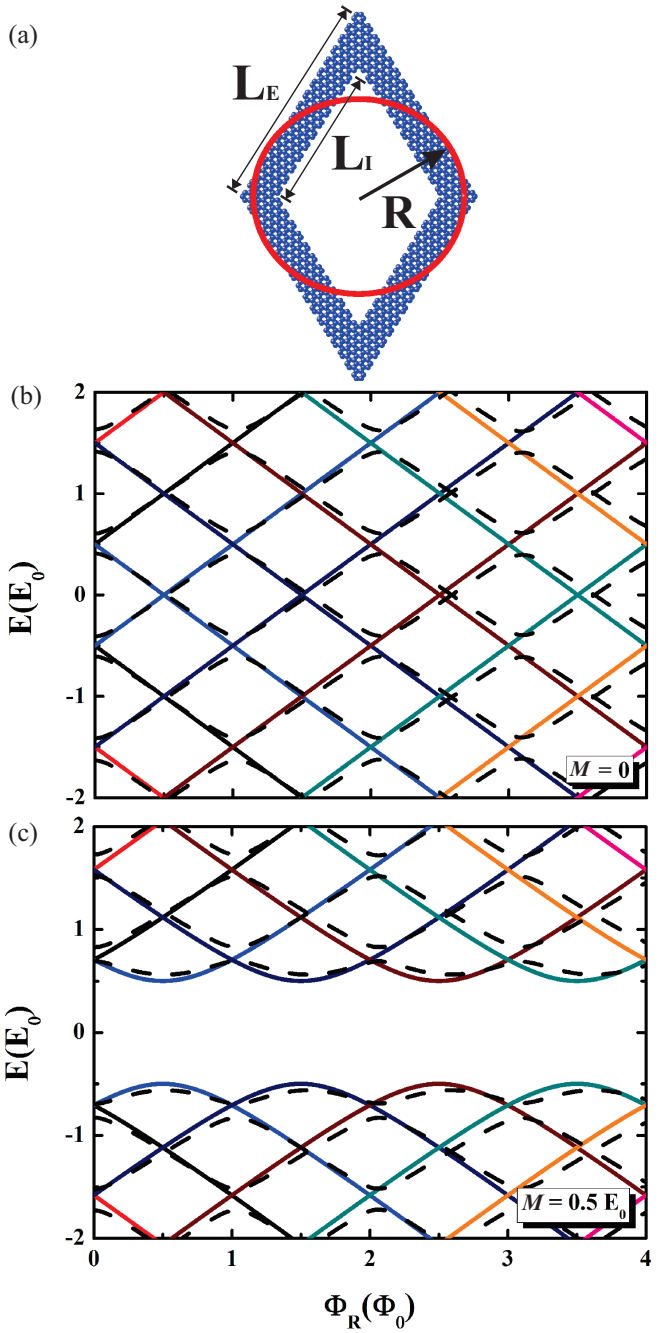

FIG. 5. (Color online) (a) Rhombus armchair quantum ring (blue polygon figure) considered in the TB calculation, with $N_E = 17$ and $N_I = 12$, along with the one-dimensional $R \approx 32.3$ Å ring (red circle) considered in the simplified model. (b) Energy spectra, obtained from the simplified (solid lines) and TB (dashed lines) models, as a function of the magnetic flux threading the red circle illustrated in (a). Curves with different colors represent different angular momentum index l. (c) The results from the TB model with a background mass term $M = 0.5E_0$ are also compared to those from the simplified model in this case.

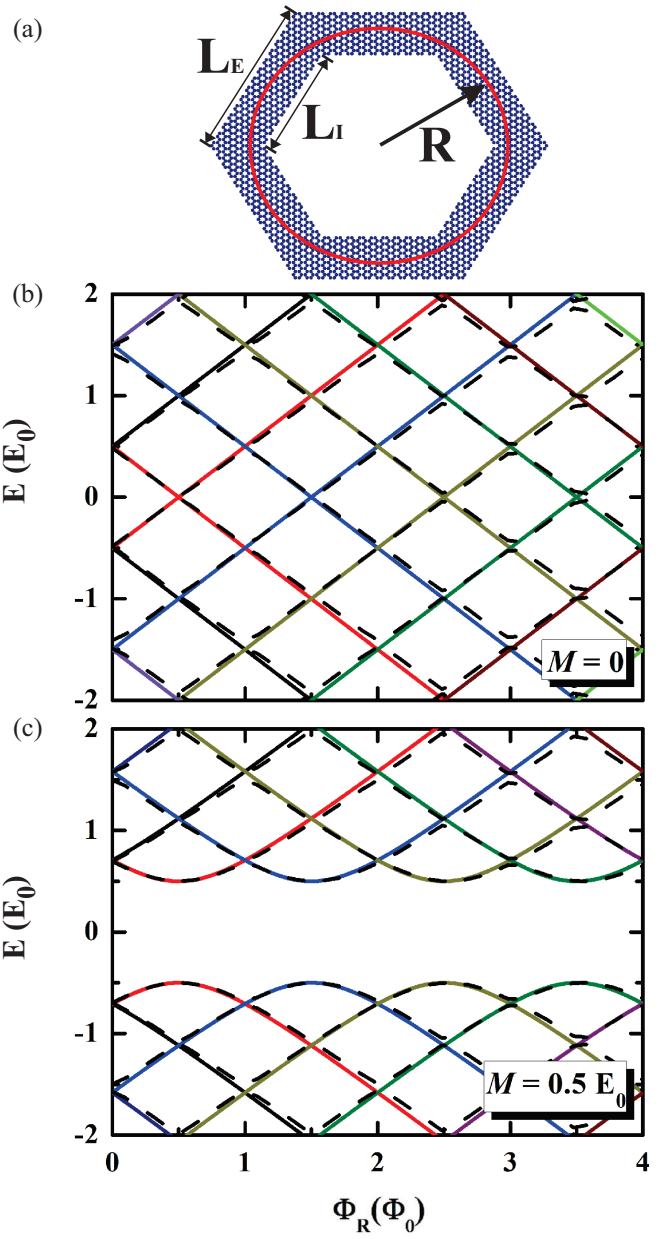

FIG. 6. (Color online) (a) Hexagonal armchair quantum ring (blue polygon figure) considered in the TB calculation, with $N_E = 15$ and $N_I = 10$, along with the one-dimensional $R \approx 47$ Å ring (red circle) considered in the simplified model. (b) Energy spectra, obtained from the simplified (solid lines) and TB (dashed lines) models, as a function of the magnetic flux threading the red circle illustrated in (a). Curves with different colors represent different angular momentum index l. (c) The results from the TB model with a background mass term $M = 0.5E_0$ are also compared to those from the simplified model in this case.

results obtained by the TBM for an armchair hexagonal ring are computed by varying the number of external carbon rings N_E, but keeping the ring width constant ($N_I = N_E - 5$), we obtain the dimensions $L_E = (3N_E - 2)a$ and $L_I = (3N_I - 1)a$ and the average radius $R = [\frac{3\sqrt{3}}{2\pi}(\frac{|L_E+L_I|}{2})^2]^{1/2}$, such that we can relate to the radius of the simplified model. The TB results are shown by the dashed lines and exhibit almost perfect agreement with the analytical results, both qualitatively and quantitatively. In both models the ground state energy would converge to $E = 0$ for large radius if it were not for the gap opened by a background mass term considered in this case,

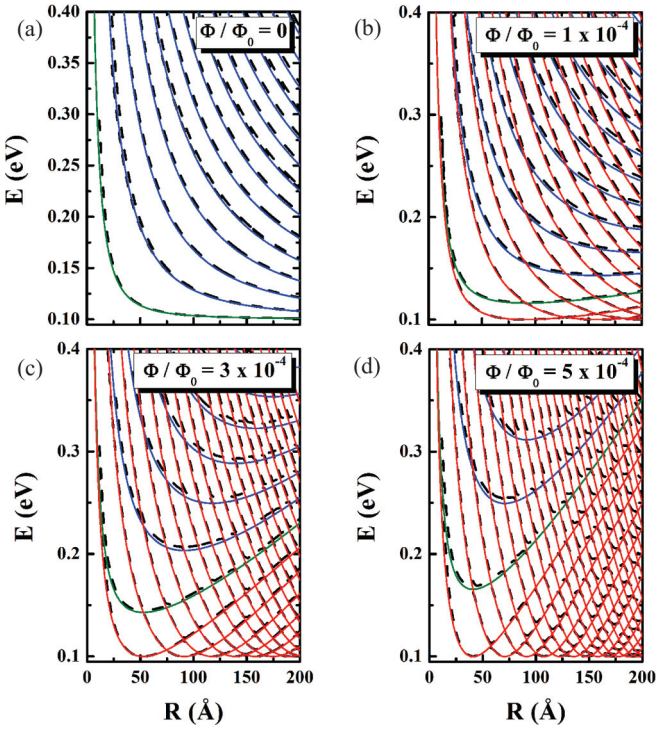

FIG. 7. (Color online) Energy levels of armchair hexagonal quantum ring, obtained from the simplified (solid line) and TB (dashed line) models, as function of ring radius R, calculated assuming an average radius given by $R = [\frac{3\sqrt{3}}{2\pi}(\frac{|L_E+L_I|}{2})^2]^{1/2}$ and mass term $M = 0.1$ eV, for different values of the magnetic flux Φ/Φ_0. Curves with green, red, and blue colors represent angular momentum index l zero, negative, and positive, respectively. The spectrum is symmetric with respect to $E = 0$.

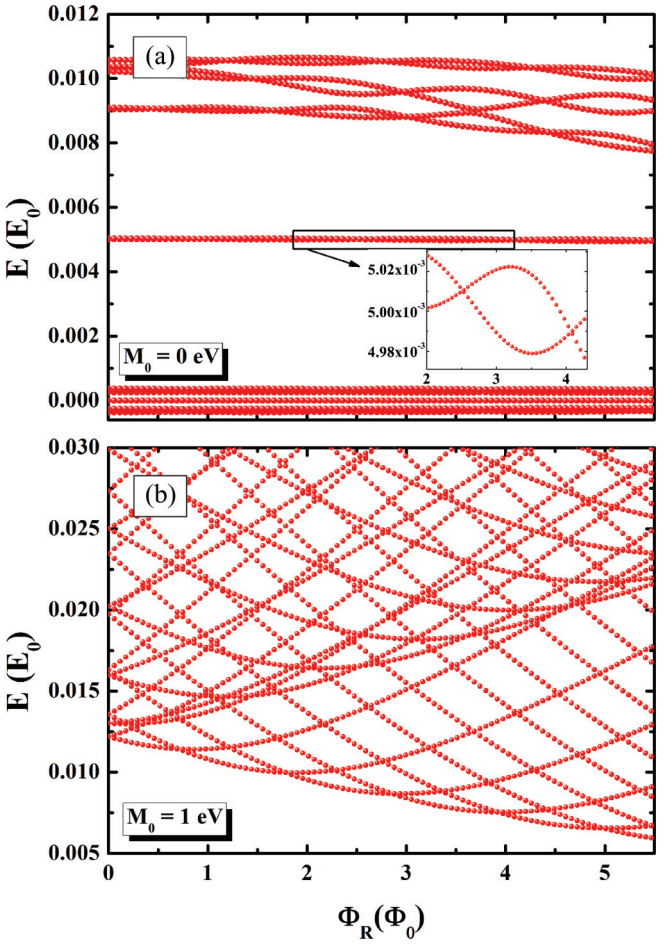

FIG. 8. (Color online) Energy levels as a function of the magnetic flux through a single carbon hexagon for (a) the circular graphene ring schematically shown in Fig. 1(g), and (b) a quantum ring formed by a site-dependent potential given by Eq. (2) and schematically shown in Fig. 1(h), with smoothness $S = 10$ Å and height $M_0 = 1$ eV. In both cases, the average radius of the ring is $R = 80$ Å and the width is 60 Å. The spectrum is symmetric with respect to $E = 0$.

which keeps electron and hole bands from touching each other even for larger radii.

It is however important to point out that the comparison between the models in Figs. 4–7 is performed for narrow widths of the quantum ring. As previously mentioned, Fig. 3(b) demonstrates that larger ring width leads to a stronger dependence of the energy spectrum on the magnetic field, which harms the similarities between the energy spectra obtained by the TBM and the Dirac model. Indeed, the armchair nature of the edges helps the electron to stay in the middle of the rings arms, since this kind of edge type does not allow for edge states, while the narrow width of the ring leads to the "frozen" motion in the radial direction, which makes systems with such narrow width more suitable to be described as an ideal ring in the simplified Dirac model proposed here.

Finally, let us now discuss how the Dirac model compares to the TBM for a finite width circular graphene ring. The difficulty in this case lies in the fact that one must consider the appropriate boundary conditions in order to properly describe the zigzag and armchair edges in this structure [44]. For the circular ring cut out from a graphene sheet, as shown in Fig. 1(g), although the circular symmetry provides an easy way to study the problem by a one-dimensional (radial) equation, the boundary conditions are still too complicated for an analytical treatment of this system, since they are an admixture of zigzag and armchair edges. The energy spectrum obtained by the TBM for the circular ring schematically illustrated in Fig. 1(g) is presented in Fig. 8(a) as a function of the magnetic flux $\Phi_R = \pi R^2 B$ threading the average ring radius $R = 80$ Å. Due to the circular symmetry, the energy bands are twofolded and exhibit AB oscillations as the magnetic flux increases, which are not perfectly periodic in Φ_R due to the finite width $W = 60$ Å of the system. The energy spectrum for a similar system was investigated in Ref. [38], but there the twofold bands are absent, which is due to the fact that the system considered in this previous work was not perfectly symmetric with respect to the y axis, as one can verify by a rigorous analysis of Fig. 7(b) in this reference. In Fig. 8(b) we present results for the mass defined circular quantum ring [11,14,16] sketched in Fig. 1(h), considering a potential height $M_0 = 1$ eV and a smooth interface $S = 10$ Å, for a ring with the same average radius and width as in Fig. 8(a). The spectrum in this case exhibits a ≈170 meV gap that decreases as the magnetic field increases, and a degenerate ground state. The magnetic field lifts the ground state degeneracy and clear AB oscillations are observed. Surprisingly, none of the

spectra found for the two circular structures investigated here within the TBM resembles the one obtained by the simplified Dirac model of a circular ring. Actually, the results from the simplified model in the presence of a background mass [see, e.g., Figs. 5(b) and 6(b)] looks qualitatively closer to the one observed in Fig. 8(b) for the mass defined ring, but some evident disparities are clearly observed, such as the strong dependence of the gap on the magnetic field, and the existence of two sets of oscillating energies, one that increases and the other that decreases as the magnetic field increases, which will be explained further on. In the case of the cut out ring [Fig. 1(g)], the different edge types play such an important role that the only evidence of the circular character of the system on the energy spectrum lies in its weak AB oscillations, and no resemblance with the simplified model spectrum for circular rings can be realized in the TBM spectrum for such a system.

On the other hand, Recher *et al.* [14] have shown that when the ring confinement is provided by a gap opened in its inner and outer regions due to an infinite mass term, an analytical solution within the Dirac model can be obtained. This solution was repeated in subsequent papers [11,16], where it was shown that the ground state energy oscillates periodically with the magnetic flux and is degenerate in the absence of a magnetic field. As the analytical solution was discussed previously in Refs. [11,14,16], we will not repeat them here, and will restrict ourselves to the discussion of the obtained results within this model. Figure 9 shows the energy spectrum, obtained within the Dirac model, for the mass defined ring in Fig. 1(h), considering the same parameters as in Fig. 8(b). The results in this case agree very well with those in Fig. 8(b), which were obtained within the TBM. Moreover, a better understanding of the TBM results is now provided by this Dirac model—the two sets of energy states that increase and decrease with the magnetic field, which are clearly observed in the TBM results in Fig. 8(b), are now demonstrated to come from the contributions of K (red solid line) and K' (blue dashed line) branches of the spectrum, and such a lifting of valley degeneracy may be important for future valleytronic devices. Hence, the development of a Dirac model that agrees well with the TBM results in this case now proves its great importance, as there would be no way to recognize such valley dependence of the energy branches only within the TBM approach.

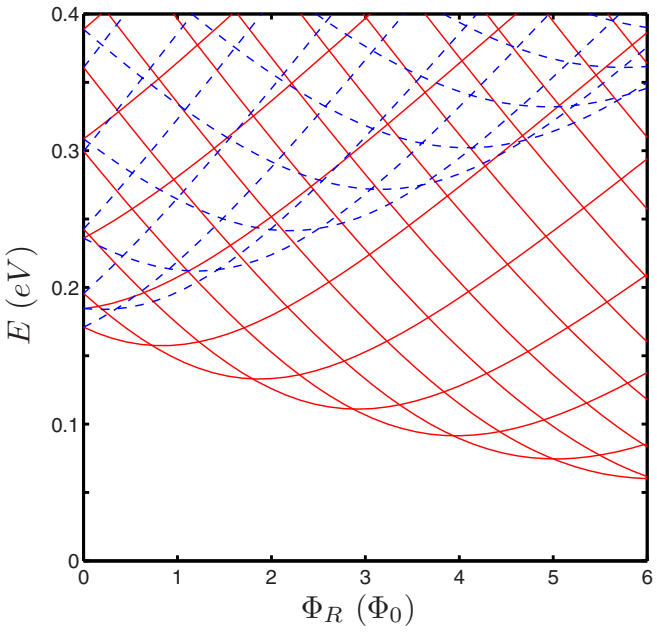

FIG. 9. (Color online) Energy spectrum, obtained by the continuum model for K (red solid line) and K' (blue dashed line), as a function of the magnetic flux for a graphene quantum ring defined by an infinite mass boundary, with the same average radius and width as the ring in Fig. 8(b). The spectrum is symmetric with respect to $E = 0$.

B. Geometry, edge types, and n-fold energy bands

Let us now discuss the energy spectra of graphene rings having different geometries and edge types, which were found to be noncompatible with the results from the Dirac models proposed here, but which display interesting similarities among each other and with previous results, besides exhibiting signatures from the symmetry of the ring, as we will demonstrate further on.

Figure 10 shows the energy spectra of zigzag hexagonal rings with $N_E = 15$ and $N_I = 10$ [Fig. 10(a)] and $N_I = 9$ [Fig. 10(b)]. Depending on the ring width, the spectrum can either exhibit a central sixfold subband around $E = 0$, as in Fig. 10(a), or two sixfold subbands separated by a gap around this energy, as shown in Fig. 10(b). A structural difference determines the qualitative behavior of the spectrum: The (former) latter is obtained when the external and internal zigzag edges of the ring are (anti-)aligned, as illustrated in the insets. Contrary to the nanoribbon case, for quantum rings it is the zigzag structure that exhibits an oscillatory behavior as the width changes. This agrees with the fact that the electronic properties of zigzag nanoribbons oriented at 120° with respect to one another, exhibit oscillatory behavior as the width changes, whereas such junctions made with armchair nanoribbons show no qualitative dependence on the width [45]. This supports the idea that the energy spectra of hexagonal graphene rings are strongly dependent on the electronic properties of their corner junctions.

Such a strong dependence on the edge type, where even the alignment of the edges play an important role, is hard to describe by analytical solutions within the continuum model. Besides, it is clear that both spectra in Fig. 10 cannot be obtained from our simplified model. Nevertheless, we can still estimate the period of the energy oscillations observed in Fig. 10 by $\Phi_R = n\Phi_0$, using a reasonable value of ring radius, which in the case of Fig. 10 is ≈29 Å. As the energy spectrum for the aligned case, shown in Fig. 10(b), exhibits a gap around $E = 0$, one could expect that introducing $M \neq 0$ in Eq. (9) would lead to the correct energy spectrum. Although the low-lying states of this spectrum resembles qualitatively those in Fig. 6(b) for $M = 0.5E_0$, the AB oscillations found by the simplified model exhibit a π-phase shift in comparison to the results in Fig. 10(b), so that the ground state for $\Phi_R = 0$ in Fig. 6(b) [Fig. 10(b)] is double (non)degenerate.

Notice that the energy spectrum of hexagonal graphene rings with zigzag edges has been previously investigated in Ref. [38], but with a different focus. In these previous results, the sixfold energy bands of this system were already pointed

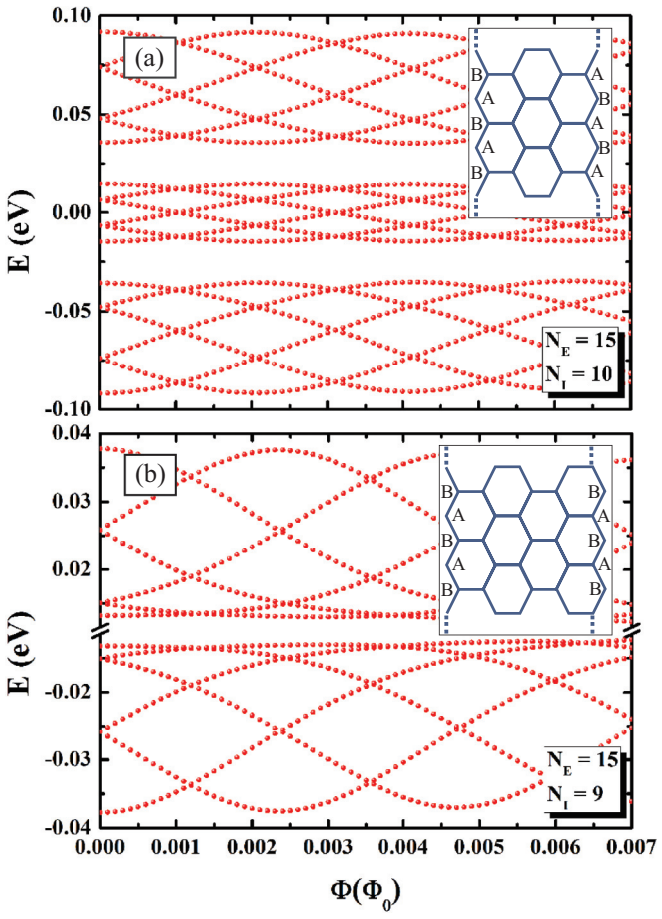

FIG. 10. (Color online) Energy levels of zigzag hexagonal quantum rings, schematically shown in Fig. 1(b), as a function of the magnetic flux through a single carbon hexagon for two ring widths: (a) $N_E = 15$, $N_I = 10$ and (b) $N_E = 15$, $N_I = 9$. In the (former) latter the inner and outer zigzag edges are (anti-)aligned, as sketched in the insets.

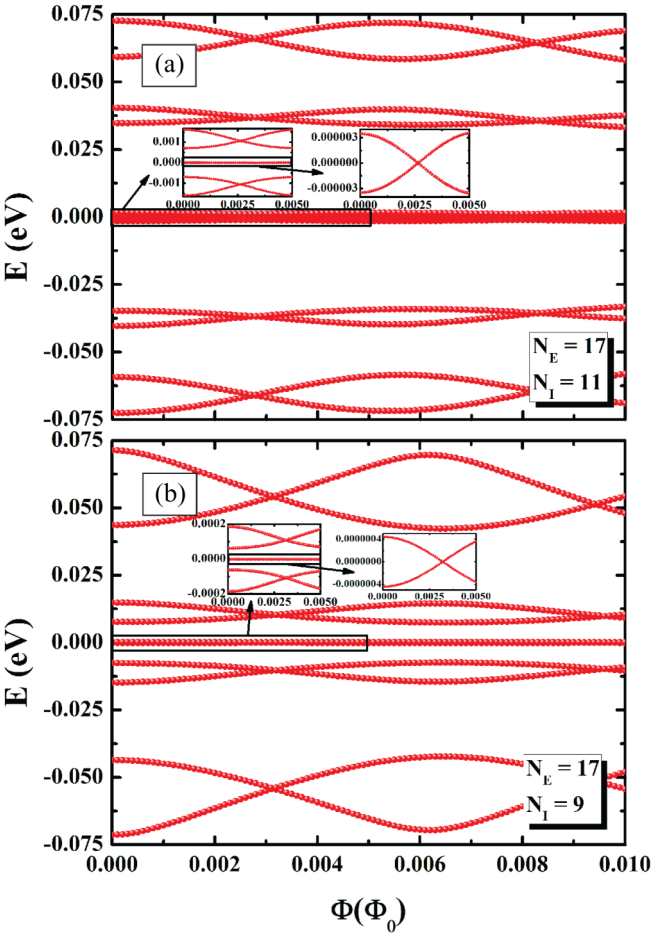

FIG. 11. (Color online) Energy levels of zigzag rhombus quantum rings, schematically shown in Fig. 1(f), as a function of the magnetic flux through a single carbon hexagon for two ring widths: (a) $N_E = 17$, $N_I = 11$ and (b) $N_E = 17$, $N_I = 9$. For both widths, the energy spectrum does not have a zero-energy state, they are three pairs of oscillating states as shown in the insets.

out. However, information about the details of the energy spectrum close to the Fermi energy and their dependence on the edges alignment, as well as the possibility of predicting the period of AB oscillations by using the Dirac model, were missing, and are now complemented by the results of the present paper.

The energy spectra of rhombus-shaped quantum rings with zigzag edges are shown in Fig. 11 as a function of the magnetic flux, for the same value of N_E as in Fig. 2 and with $N_I = 11$ [Fig. 11(a)] and $N_I = 9$ [Fig. 11(b)]. In this case, due to the geometry of the system, it is not possible to construct zigzag rhombus rings having different kinds of edges alignment. In this way, the spectra for different ring widths exhibit the same qualitative behavior, with twofold energy subbands, just like those previously observed for the armchair case in Fig. 2. Notice that the states around $E = 0$, that look like zero-energy states, are rather composed by three pairs of oscillating states, with very low energy. As a matter of fact, the twofold energy bands of this system have been already pointed out by Bahamon *et al.* [38], therefore our results complement the findings of this previous paper by providing details of the energy spectrum around $E = 0$, as well as the dependence of the energy spectrum on the ring width.

Figure 12 shows the energy spectra for triangular zigzag quantum rings considering two ring sizes: (a) $N_E = 17$, $N_I = 12$ and (b) $N_E = 15$, $N_I = 10$. Just like the zigzag rhombus case, the zigzag triangular rings can only be constructed with aligned edges. The spectra look qualitatively similar to those observed for the zigzag rhombus-shaped ring in Fig. 11, but with threefold oscillating energy bands for higher energy states, instead of the pairs of oscillating states observed in the rhombus-shaped zigzag case. However, there are two important differences between these two spectra: (i) The zigzag triangular rings, in fact, exhibit zero-energy (edge) states, no matter the length of its sides, whereas zigzag rhombus-shaped rings do not, as shown by the insets of Fig. 11 and previously explained in the text. (ii) The first energy state in the zigzag rhombus-shaped ring is always nondegenerate, whereas this state in the zigzag triangular ring is doubly degenerate. Results in previous papers [38] demonstrate that the anticrossings separating the threefold energy bands of

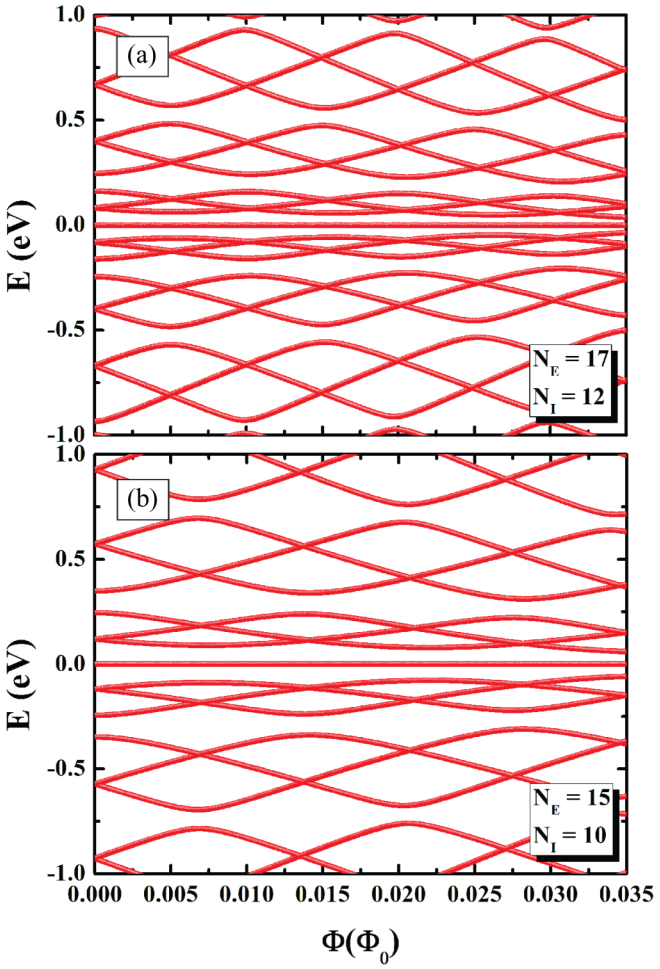

FIG. 12. (Color online) Energy levels of zigzag triangular quantum rings, schematically shown in Fig. 1(d), as a function of the magnetic flux through a single carbon hexagon for two ring widths: (a) $N_E = 17$, $N_I = 12$ and (b) $N_E = 15$, $N_I = 10$. For both widths, the energy spectrum has a zero-energy state.

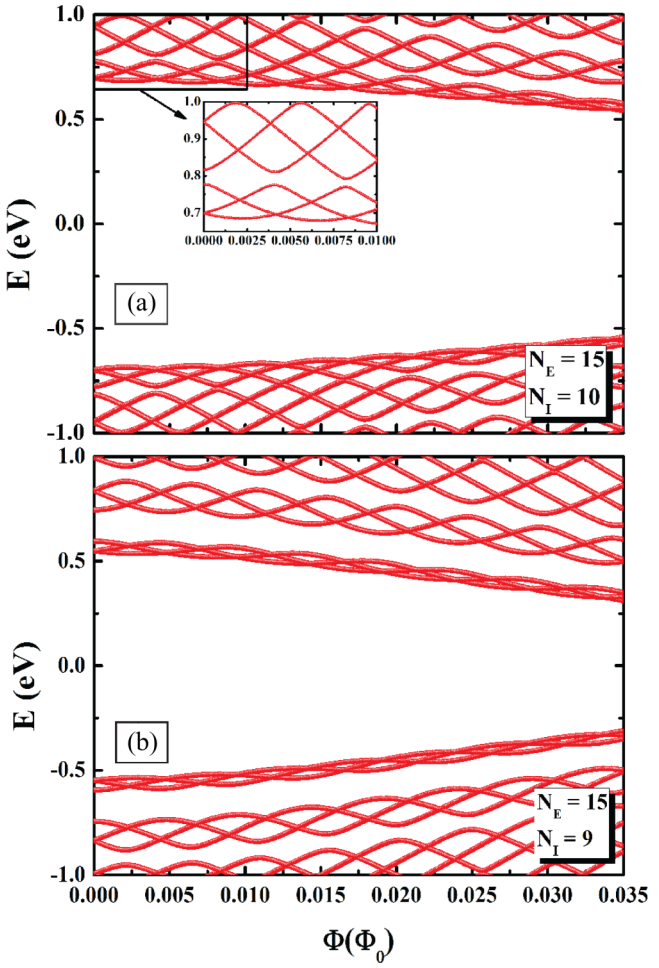

FIG. 13. (Color online) Energy levels of armchair triangular quantum rings, schematically shown in Fig. 1(c), as a function of the magnetic flux through a single carbon hexagon for two ring widths: (a) $N_E = 15$, $N_I = 10$ and (b) $N_E = 15$, $N_I = 9$. The spectrum is symmetric with respect to $E = 0$.

triangular zigzag quantum rings originate from the coupling between inner and outer edge states.

The magnetic field dependence of the energy levels of armchair triangular quantum rings is shown in Fig. 13 for (a) anti-aligned and (b) aligned edges, where the spectra are also composed by threefold oscillating energies, as in the zigzag case. However, the energy levels are shown to be much more affected by the magnetic field threading the ring in the armchair case and no significant difference on the edges alignment was observed. Another difference as compared to the zigzag triangular rings is the absence of the zero-energy state, which is expected, since the zero-energy states are normally related to edge states in zigzag boundaries [46,47]. The spectra also exhibit a huge gap of $\Delta E > 1$ eV around $E = 0$, which becomes smaller either as the magnetic field increases or as the ring width becomes larger (i.e., as N_I becomes smaller for a fixed N_E).

It is important to emphasize a clear similarity between the results obtained in the previous subsection for armchair hexagonal (rhombus-shaped) rings in Fig. 3 (Fig. 2) and those obtained for the zigzag case in Fig. 10 (Fig. 11): For any edge type or alignment, the energy spectra exhibit sixfold (twofold) energy bands, with AB oscillations with varying magnetic field. A similar effect is also shared by zigzag and armchair triangular rings, as shown in Figs. 12 and 13, respectively, where the energy spectra exhibit threefold bands. These results strongly suggest that the number of energy states composing these bands is related to the symmetry groups of rotation C_6, C_2, and C_3, for hexagon, rhombus, and triangle, respectively, which are closely related to the number of sides of the polygon formed by the ring [38].

V. CONCLUSION

We calculated the energy levels of graphene quantum rings with several geometries under an applied magnetic field and observed that the energy spectrum and the AB oscillations for these systems are strongly dependent on their geometry and edge structures. For rings with zigzag edges, the TB spectra for each geometry are qualitatively different, showing six-, three-, and twofold energy subbands, separated by large gaps, for hexagonal, triangular, and rhombuslike rings, respectively.

In the hexagonal case, the alignment between inner and outer zigzag edges is demonstrated to play an important role in the formation of the subbands, whereas the triangular and rhombus rings have only the aligned edge case due to geometric reasons, presenting similar energy spectra for different sizes. Such a strong dependence of the energy spectrum on the edge structure, specially the observed oscillatory behavior of the spectra with changing ring width, due to the alignment or anti-alignment of the inner and outer edges, is a feature of the quantum ring spectra that can hardly be captured by the continuum models.

The energy spectrum obtained from the TB model for hexagonal quantum rings with armchair edges exhibits sixfold subbands separated by narrow gaps, which become larger as the width of the ring increases. The spectrum does not have $E = 0$ states at zero magnetic field, but exhibits such states for certain values of magnetic flux. Similar features are observed for a rhombuslike ring with armchair edges (except for the sixfold subbands which, in this case, are twofold), but only in the case where the inner and outer edges are anti-aligned. The main features of these energy spectra can be obtained by a simplified model, which considers electrons obeying the Dirac equation for a circular ring with zero width. Despite the different geometry of the actual rings, with such a simple circular model one can (i) estimate the energy levels and the period of AB oscillations or, alternatively, estimate the ring radius by analyzing its energy spectrum as a function of the magnetic field, even in the presence of a substrate induced staggered potential, which appears in the continuum model as a background mass term. (ii) Predict the alternating direction of the persistent currents through the ring arms as the magnetic field increases, observed in the TBM. (iii) Predict the almost linearly increasing energy states as a function of the ring radius in the presence of an uniform magnetic field, which is also confirmed by the TBM results. The approximation is better suited for rings with smaller widths and for lower energies and magnetic fields. On the other hand, all the results for the triangular geometry in the armchair case exhibit threefold subbands separated by large energy gaps, which cannot be described by such a simplified model.

We also studied two cases of circular rings within the TB model: In the first one, where the ring is cut from a graphene layer, we observe an energy spectrum composed by pairs of energy states which exhibit AB oscillations as the magnetic field increases. In the second, where the electrons are confined in a ringlike structure by an external staggered site-dependent potential, the energy spectrum exhibits a gap around $E = 0$ and the ground state is doubly degenerate in the absence of a magnetic field. As the magnetic field increases, this degeneracy is lifted, the energy gap is reduced, and AB oscillations are observed in two different branches of energies, one that increases and the other that decreases with magnetic field. Surprisingly, the TBM results for both *circular* cases are very different from those obtained by the simplified continuum model for a *circular* ring, which, in turn, was demonstrated to perfectly describe *hexagonal* and *rhombuslike* armchair rings. On the other hand, our results demonstrate that the spectrum of the staggered potential case can be obtained by the continuum model for a finite width circular ring defined by mass barriers, where one identifies the different energy branches observed in the TBM results as coming from different Dirac cones, demonstrating a magnetic field induced lifting of the valley degeneracy in these systems. However, the mass boundary conditions used here and in Refs. [11,14,16] are shown to describe only the case of a ring defined by a ringlike staggered potential, so that the complicated energy spectrum of the more realistic circular ring cut out of a graphene sheet cannot be described by any of the simplistic boundary conditions or simplified models analyzed here.

We thus summarize our findings with the following general conclusions: (1) rings with a given n-fold symmetry exhibit n-fold energy subbands; (2) edge alignment in zigzag hexagonal rings lead to differences in the sixfold subbands distribution around the Fermi level, whereas for armchair rhombus-shaped rings, drastic modifications to the energy spectrum are observed, specially regarding the separation between the twofold bands; (3) an infinitely thin Dirac ring describes quite well armchair hexagonal and rhombus-shaped (with anti-aligned edges) structures, specially for thin ring widths; and (4) the Dirac model for a ring defined by infinite mass boundaries does not describe rings cut out of a graphene flake, but rather those defined by a ring-shaped staggered potential.

ACKNOWLEDGMENTS

This work was financially supported by CNPq, under Contract NanoBioEstruturas 555183/2005-0, PRONEX/FUNCAP, CAPES Foundation under the process number BEX 7178/13-1, the Bilateral programme between CNPq and the Flemish Science Foundation (FWO-Vl), and the Brazilian Program Science Without Borders (CsF).

[1] K. S. Novoselov, A. K. Geim, S. V. Morozov, D. Jiang, Y. Zhang, S. V. Dubonos, I. V. Grigorieva, and A. A. Firsov, Science **306**, 666 (2004).

[2] A. H. Castro Neto, F. Guinea, N. M. R. Peres, K. S. Novoselov, and A. K. Geim, Rev. Mod. Phys. **81**, 109 (2009).

[3] Z. Wu, Z. Z. Zang, K. Chang, and F. M. Peeters, Nanotechnology **21**, 185201 (2010).

[4] M. Zarenia, A. Chaves, G. A. Farias, and F. M. Peeters, Phys. Rev. B **84**, 245403 (2011).

[5] M. Grujić, M. Zarenia, A. Chaves, M. Tadić, G. A. Farias, and F. M. Peeters, Phys. Rev. B **84**, 205441 (2011).

[6] P. Hewageegana and V. Apalkov, Phys. Rev. B **77**, 245426 (2008).

[7] C. A. Downing, D. A. Stone, and M. E. Portnoi, Phys. Rev. B **84**, 155437 (2011).

[8] J. Schelter, B. Trauzettel, and P. Recher, Phys. Rev. Lett. **108**, 106603 (2012).

[9] S. Zhang, H. Chen, E. Zhang, and D. Liu, Europhys. Lett. **103**, 58005 (2013).

[10] J. Schelter, D. Bohr, and B. Trauzettel, Phys. Rev. B **81**, 195441 (2010).
[11] C.-H. Yan and L.-F. Wei, J. Phys.: Condens. Matter **22**, 295503 (2010).
[12] S. Russo, J. B. Oostinga, D. Wehenkel, H. B. Heersche, S. S. Sobhani, L. M. K. Vandersypen, and A. F. Morpurgo, Phys. Rev. B **77**, 085413 (2008).
[13] T. Luo, A. P. Iyengar, H. A. Fertig, and L. Brey, Phys. Rev. B **80**, 165310 (2009).
[14] P. Recher, B. Trauzettel, A. Rycerz, Ya. M. Blanter, C. W. J. Beenakker, and A. F. Morpurgo, Phys. Rev. B **76**, 235404 (2007).
[15] J. Wurm, M. Wimmer, H. U. Baranger, and K. Richter, Semicond. Sci. Technol. **25**, 034003 (2010).
[16] D. S. L. Abergel, V. M. Apalkov, and T. Chakraborty, Phys. Rev. B **78**, 193405 (2008).
[17] M. Zarenia, J. M. Pereira, A. Chaves, F. M. Peeters, and G. A. Farias, Phys. Rev. B **81**, 045431 (2010); **82**, 119906 (2010).
[18] F. E. Meijer, A. F. Morpurgo, and T. M. Klapwijk, Phys. Rev. B **66**, 033107 (2002); B. Molnár, F. M. Peeters, and P. Vasilopoulos, *ibid.* **69**, 155335 (2004).
[19] T. García, S. Rodríguez-Bolívar, N. A. Cordero, and E. Romera, J. Phys.: Condens. Matter **25**, 235301 (2013).
[20] M. I. Katsnelson, K. S. Novoselov, and A. K. Geim, Nat. Phys. **2**, 620 (2006).
[21] A. Matulis and F. M. Peeters, Phys. Rev. B **77**, 115423 (2008).
[22] J. Wurm, A. Rycerz, I. Adagideli, M. Wimmer, K. Richter, and H. U. Baranger, Phys. Rev. Lett. **102**, 056806 (2009).
[23] S. Schnez, K. Ensslin, M. Sigrist, and T. Ihn, Phys. Rev. B **78**, 195427 (2008).
[24] S. Y. Zhou, G.-H. Gweon, A. V. Fedorov, P. N. First, W. A. de Heer, D.-H. Lee, F. Guinea, A. H. Castro Neto, and A. Lanzara, Nat. Mater. **6**, 770 (2007).
[25] G. Giovannetti, P. A. Khomyakov, G. Brocks, P. J. Kelly, and J. van den Brink, Phys. Rev. B **76**, 073103 (2007).
[26] M. Zarenia, O. Leenaerts, B. Partoens, and F. M. Peeters, Phys. Rev. B **86**, 085451 (2012).
[27] R. E. Peierls, Z. Phys. **80**, 763 (1933).
[28] J. M. Luttinger, Phys. Rev. **84**, 814 (1951).
[29] D. R. da Costa, A. Chaves, G. A. Farias, L. Covaci, and F. M. Peeters, Phys. Rev. B **86**, 115434 (2012).
[30] A. Chaves, L. Covaci, Kh. Yu. Rakhimov, G. A. Farias, and F. M. Peeters, Phys. Rev. B **82**, 205430 (2010).
[31] J. M. Pereira, A. Chaves, G. A. Farias, and F. M. Peeters, Semicond. Sci. Technol. **25**, 033002 (2010).
[32] M. V. Berry and R. J. Mondragon, Proc. R. Soc. London Ser. A **412**, 53 (1987).
[33] In the K' point, substituting $\vec{\sigma} \rightarrow \vec{\sigma}^*$(see, e.g., Ref. [2]), one obtains the same energy spectrum, but for $l \rightarrow l + 1$.
[34] G. Paz, Eur. J. Phys. **22**, 337 (2001).
[35] A. G. Aronov and Y. B. Lyanda-Geller, Phys. Rev. Lett. **70**, 343 (1993).
[36] Y. S. Yi, T. Z. Qian, and Z. B. Su, Phys. Rev. B **55**, 10631 (1997).
[37] T. Choi, S. Y. Cho, C. M. Ryu, and C. K. Kim, Phys. Rev. B **56**, 4825 (1997).
[38] D. A. Bahamon, A. L. C. Pereira, and P. A. Schulz, Phys. Rev. B **79**, 125414 (2009).
[39] L. Brey and H. A. Fertig, Phys. Rev. B **73**, 235411 (2006).
[40] G. A. Farias, M. H. Degani, J. A. K. Freire, J. Costa e Silva, and R. Ferreira, Phys. Rev. B **77**, 085316 (2008).
[41] A. C. A. Ramos, A. Chaves, G. A. Farias, and F. M. Peeters, Phys. Rev. B **77**, 045415 (2008).
[42] A. Chaves, J. Costa e Silva, J. A. K. Freire, and G. A. Farias, Microelect. J. **39**, 455 (2008).
[43] E. A. de Andrada e Silva, Am. J. Phys. **60**, 753 (1992).
[44] A. R. Akhmerov and C. W. J. Beenakker, Phys. Rev. B **77**, 085423 (2008).
[45] A. Iyengar, T. Luo, H. A. Fertig, and L. Brey, Phys. Rev. B **78**, 235411 (2008).
[46] P. Potasz, A. D. Guclu, O. Voznyy, J. A. Folk, and P. Hawrylak, Phys. Rev. B **83**, 174441 (2011).
[47] P. Potasz, A. D. Guclu, and P. Hawrylak, Phys. Rev. B **81**, 033403 (2010).